Zhao, Wenli; Han, Bing; Jakobsson, Kaj; Louhi-Kultanen, Marjatta; Alopaeus, Ville

Mathematical model of precipitation of magnesium carbonate with carbon dioxide from the magnesium hydroxide slurry

Published in:
Computers and Chemical Engineering

DOI:
10.1016/j.compchemeng.2016.01.013

Published: 06/04/2016

Document Version
Peer-reviewed accepted author manuscript, also known as Final accepted manuscript or Post-print

Mathematical model of precipitation of magnesium carbonate with carbon dioxide from the magnesium hydroxide slurry

Wenli Zhao[a,*], Bing Han[b], Kaj. Jakobsson[a], Marjatta Louhi-Kultanen[b], Ville Alopaeus[a]

[a] *Aalto University, School of Chemical Technology, P.O.Box 16100, FI-00076 Aalto, Finland*

[b] *Lappeenranta University of Technology, Department of Chemical Technology, P.O.Box 20, FI-53851, Finland*

Abstract

A mathematical model is proposed for a precipitation process of magnesium carbonate in a heterogeneous stirred tank reactor. The model includes a description of dissolution of $Mg(OH)_2$, absorption of CO_2 and precipitation of $MgCO_3$. The Nernst-Planck equation is used in the dissolution model to maintain the mass balance and electroneutrality. The van Krevelen–Hoftijzer expression is introduced to describe the enhancement effect of reaction between dissolved CO_2 and OH^- on the mass transfer rate of dissolution and absorption. In the precipitation model, a simplified population balance equation is solved by a moment method for both dissolving and precipitating particles. Unknown precipitation kinetics parameters for $Mg(OH)_2$-$MgCO_3$ system are fitted against experimental data and compared with $Ca(OH)_2$-$CaCO_3$ system. According to the present analysis, the liquid-solid and gas-liquid mass transfer dominate the global rate of precipitation. The precipitation kinetics and pH have strong influences on the concentration of reactants and the yield of precipitation.

Keywords: Mass transfer modeling; Dissolution; Absorption; Precipitation; Nernst-Planck; Heterogeneous reaction

* Corresponding author. Tel.: +358 45 1674316
E-mail address: wenli.zhao@aalto.fi
Present address: Aalto University, School of Chemical Technology P. O. Box 16100, FI-00076, Finland

1. Introduction

With increasing carbon levels in the atmosphere, carbon dioxide (CO_2) capture and storage are gradually regarded as a significant approach to avoid the potentially devastating consequences of global warming and climate change. Mineral carbonation is considered as one of the most efficient technologies where a reaction between CO_2 and alkaline-minerals forms carbonates. The mineral carbonation is a complex chemical process including not only chemical reaction but also precipitation.

Precipitation refers to the unit operation both in the manufacturing of solid materials and in the separation of chemical components with varying solubilities or melting points (Mullin, 2001). Here we consider the precipitation process taking place in a stirred tank reactor. To model the precipitation process from a heterogeneous solution is not a trivial modelling task. The quality of the simulation depends on the accurate precipitation kinetics modelling and appropriate fluid field prediction (Jones et al., 2005). Along with the increasing computing power, several precipitation models combined with fluid field calculation have been published over the past decade (Wei and Garsude, 1997; Al-Rashed and Jones, 1999; Cheng et al., 2012). These studies led to a better understanding of mechanisms for precipitation. The overall kinetic model of the solid-gas-liquid precipitation, however, has remained relatively unexplored until now due to the complicated mechanism including simultaneous dissolution, absorption and precipitation.

As the first step of precipitation, the reactive dissolution is widely studied in leaching processes and solid–liquid catalyzed reactions, such as in production of terephthaloyl chloride and alkylation of the potassium salts of carboxylic acids (Sidorov et al., 1986). The reactive dissolution of a solid in a liquid solution mainly contains two steps: a reaction at the solid-liquid interface and a diffusion of the dissolving component towards the bulk solution (Dokoumetzidis et al., 2006; Macheras and Iliadis, 2006). The slower step has a dominating influence upon the rate of dissolution. The diffusion control is typically hypothesized under the condition of fast surface reaction (Noyes and Whitney, 1897; Khoury et al., 1988; Missel et al., 2004a, 2004b). As the interface concentration is impossible to measure, the equilibrium concentration calculated

from the solubility product is typically used in the mass transfer model models describing the phenomena. The classical assumption treats each ion individually and does not necessarily satisfy even the basic constraints, such as electroneutrality. In order to revise the defect in the above assumption, the Nernst-Planck equation has been introduced into the mass transfer model in the electrolyte solution. The Nernst-Planck equation describes the flux of ions under the influence of both ionic concentration gradient and electric field (Newman, 1991). It can also extend Fick's law of diffusion for the case where the diffusing particles are also moving with respect to the fluid by electrostatic forces. In addition, the dissolution of solids is enhanced by a second order reaction between carbon dioxide and hydroxide ion in the liquid film near solid-liquid interface (Uchida et al., 1975). The shrinking diameter of dissolving particle has significant influence on the solid-liquid mass transfer coefficient and mass transfer area as well.

In the absorption processes where CO_2 is one of the reagents, the mass transfer between gas and liquid phases could become the rate limiting step. Therefore accurate modelling of the absorption process is also needed (Ramachandran and Sharma, 1969; Sada et al., 1977; Velts et al., 2011; Lin et al., 2006). Models of these studies mentioned above can be directly used when building a comprehensive model for a heterogeneous precipitation.

As the final step of the precipitation process, the formation of the precipitated particles should be predicted. This is best done by the population balance equation (PBE) in company with material balances and the kinetics model of precipitation. The PBE can be solved with various numerical methods which are classified into four main categories: classes methods, moment methods, weighted residuals methods and stochastic methods. Moment methods transform the PBE from partial differential equations (PDEs) into a set of ordinary differential equations (ODEs) of low-order moments. Although the precise shape of the CSD is lost, the low-order moments contain most of the useful information, such as number, surface area, volume and mean particle size depending on the moments selected to be resolved (Wang and Fox, 2003).

Regarding to the reaction mechanism, the complex interaction between mass transfer, chemical reaction and precipitation needs to be considered (Sada et al., 1988; Wachi and Jones, 1991a, 1991b; Jones et al., 1992). Unfortunately, no such model exists for precipitation of $MgCO_3$ in the literature. In this paper, the dissolution, absorption and precipitation were first analyzed individually and then combined to build a holistic precipitation model. The relevant kinetics parameters were furthermore fitted against available experimental data (Han et al., 2014a, 2014b). The proposed model is capable of predicting precipitation process performance in cases where the rate controlling step may vary (Lin et al., 2006). This is highly preferable in scale-up and in cases where the raw material or product property demands are changed.

2 The Mathematical Model

In the precipitation model, the mass transfer with chemical reaction in gas-liquid absorption and the population balance equation in precipitation are generally described by PDEs. In order to simplify the model and to transform PDEs into ODEs, the following assumptions are made:

1. The reactant particles are of uniform size and spherical. The liquid volume is assumed to be constant. The reference volume for the specific area of particles and bubbles is the total volume of dispersion (gas, solids, and continuous liquid).

2. Only ions of Mg^{2+}, H^+ and OH^- are involved in the dissolution model. The dissolution rate of $Mg(OH)_2$ is controlled by the mass transfer between solid-liquid interface and bulk solution. The interface concentration is at equilibrium (Lin et al., 2006).

3. The absorption and precipitation in liquid film adjacent to the gas-liquid interface are neglected. The model assumes that the gas absorption and precipitation only occur in the bulk solution (Jones et al., 1992).

4. The nucleation and crystal growth rate can be expressed as power-law functions of the supersaturation in the bulk solution. The crystal growth rate is taken to be independent of crystal size.

5. Aggregation and breakage of the precipitated crystals are neglected.

6. Prefect micro-mixing and macro-mixing are assumed in the stirred tank.

2.1 Dissolution Model

The rate of dissolution is assumed to be controlled by mass transfer of the dissolving solids away from the solid-liquid interface (Bhaskarwar, 1988; Hsu et al., 1991; Riazi and Faghri, 1985; Rice and Jonea, 1979). A shrinking-particle model has been found suitable for describing the dissolution reaction of a nonporous sphere and is adopted here (Levenspiel, 2007). The dissolution scheme is described as follows:

$$\mathrm{Mg(OH)_2(s)} \leftrightarrow \mathrm{Mg^{2+} + 2OH^-} \tag{1}$$

The flux between the solid-liquid interface and bulk is used to calculate the mass transfer rate in Eq. (2):

$$dc_i / dt = \alpha_S N_i V_{disp} / V_L \tag{2}$$

$$V_{disp} = V_L + V_g + V_s \tag{3}$$

where c_i are the concentration of components i, mol·m^{-3}; N_i are the flux between solid-liquid interface and bulk solution, mol·m^{-2}·s^{-1}; α_S is the specific area for the mass transfer, m^2/m^3; V_{disp} is the total volume of

dispersion system, m^3; V_L is the volume of liquid, m^3; V_G is the average volume of gas, m^3; V_S is the total volume of $Mg(OH)_2$ and $MgCO_3$, m^3.

According to the assumption 1 stated earlier, total number of dissolving particles N_{tot} is constant. The total particle surface area can be calculated as follows:

$$A = \alpha_S V_{disp} = \pi d_p^{\ 2} N_{tot} \tag{4}$$

$$d_p = \sqrt{\frac{\alpha_S V_{disp}}{\pi N_{tot}}} \tag{5}$$

where A is the total mass transfer area, m^2; d_p is the average diameter of the dissolving particle, m.

Therefore the total amount of $Mg(OH)_2$ and the specific mass transfer area of the dissolving solids are calculated as follows:

$$n_{Mg(OH)_2} = \frac{\pi d_p^{\ 3} N_{tot} \rho_{Mg(OH)_2}}{6 M_{Mg(OH)_2}} = \frac{\alpha_S^{\ 1.5} \rho_{Mg(OH)_2}}{6\pi^{0.5} N_{tot}^{\ 0.5} M_{Mg(OH)_2}} V_{disp}^{\ 1.5} \tag{6}$$

$$\alpha_S = \left(\frac{6\pi^{0.5} N_{tot}^{\ 0.5} n_{Mg(OH)_2} M_{Mg(OH)_2}}{\rho_{Mg(OH)_2} V_{disp}^{\ 1.5}} \right)^{2/3} \tag{7}$$

where $n_{Mg(OH)2}$ is the total amount of $Mg(OH)_2$, mol; $M_{Mg(OH)2}$ is the molar mass of $Mg(OH)_2$, $kg \cdot mol^{-1}$; $\rho_{Mg(OH)2}$ is the density of $Mg(OH)_2$, $kg \cdot m^{-3}$.

According to the Nernst-Planck equation, the flux between interface and bulk solution, N_i, is the sum of migration, diffusion and convection of electrolyte (Newman, 1991):

$$N_i = -z_i \frac{D_i}{RT} F \bar{c}_i \nabla \phi - D_i \nabla c_i + \bar{c}_i v \tag{8}$$

In dilute nonelectrolyte solutions, species diffuse independently according to their concentration gradient and diffusion coefficient. However, in electrolyte solutions solutes do not diffuse independently. The diffusion potential exists in the solution due to the current which is calculated as:

$$I = F\sum_i (z_i N_i) = -F^2 \nabla \phi \sum_i (z_i^{\,2} \frac{D_i}{RT} \bar{c}_i) - F\sum_i (z_i D_i \nabla c_i) + F\sum_i (z_i \bar{c}_i v) \tag{9}$$

In the case of no electric current, such as in mass transfer between electrically neutral particles and surrounding liquid, the current (I) must be zero. Also the convection term (last one on the right hand side) is zero due to electroneutrality in the liquid phase. After reorganizing the equation, the flux between interface and bulk solution is related as:

$$N_i = z_i \frac{D_i}{RT} \bar{c}_i \left[\frac{\sum_i (z_i D_i \nabla c_i)}{\sum_i (z_i^{\,2} D_i \bar{c}_i)} \right] - D_i \nabla c_i \tag{10}$$

Under the homogenous mixing assumption, all mass transfer resistances are assumed in the liquid film. Linear concentration profiles are assumed in the liquid (Ala-Kaila, 1998):

$$\nabla c_i \approx \frac{\Delta c}{\delta} = \frac{c^i - c^b}{\delta} \tag{11}$$

where δ is the thickness of the liquid film, m; c^i is the concentration of components at the interface, mol·m^{-3}; c^b is the concentration of components in the bulk solution, mol·m^{-3}.

Average concentration in the liquid film is:

$$\overline{c_i} = \frac{c^i + c^b}{2} \tag{12}$$

The correlation between diffusion coefficient D_i and convective mass transfer coefficient $k_{s,i}$ is:

$$k_{s,i} = \frac{D_i}{\delta} \tag{13}$$

After combining the equations, the final expression of flux between interface and bulk solution is written as:

$$N_i = k_{s,i}\Delta c_i - k_{s,i} z_i \overline{c_i}\left[\frac{\sum_i (z_i k_{s,i}\Delta c_i)}{\sum_i (z_i^{\,2} k_{s,i}\overline{c_i})}\right] \tag{14}$$

where $k_{s,i}$ is the solid-liquid mass transfer coefficient, $m \cdot s^{-1}$.

The first term on the right side of Eq. (14) is the typical expression of mass transfer rate in non-electrolyte solutions. The second term is the contribution of Nernst-Planck equations due to electroneutrality and zero electric current. This part ensures that the calculated mass transfer fluxes always fulfill zero current assumption.

The mass transfer coefficient is not only determined by the mixing condition and geometry of the impeller but also by the diameter of dissolving particle (Beenackers and Vanswaj, 1993). For the fine particles, $k_{s,i}$ is calculated as (Asai et al., 1989):

$$N_{Sh} = [2^{5.8} + (0.61 N_{\mathrm{Re}}^{\;0.58} N_{Sc}^{\;1/3})^{5.8}]^{1/5.8} \tag{15}$$

where N_{Sh} is the dimensionless Sherwood number; N_{Re} is the Reynolds number; and N_{Sc} is the Schmidt number.

2.2 Absorption Model

The physical dissolution of gaseous CO_2 at ambient temperature and pressure could become the rate controlling step when the dissolution rate of small reactant solids becomes very fast at the end of the precipitation. As the gas feed is pure CO_2, its concentration in gas phase is assumed to be constant, determined by the pressure and temperature. Hence the equilibrium concentration of CO_2 in liquid phase at gas-liquid interface is constant as well. It can be calculated by Henry's law. Thus the flux of CO_2 (l) between gas and liquid phase becomes:

$$N_{CO_2} = k_L\left[\left(\frac{H_{CO_2-H_2O}M_{CO_2}\left[CO_2(g)\right]_{IN}P}{\rho_{CO_2}}\right)-\left[CO_2(l)\right]\right] \tag{16}$$

where N_{CO2} is the flux of CO_2(l) between gas and liquid phase, mol·m^{-2}·s^{-1}; k_L is the gas-liquid mass transfer coefficient, m·s^{-1}; $H_{CO2\text{-}H2O}$ is the Henry's constant for carbon dioxide in water, mol· m^{-3}·atm^{-1}; M_{CO2} is the molar mass, kg·mol^{-1}; $[CO_2(g)]_{IN}$ is the concentration of the inflow gas which depends on the temperature and pressure, mol· m^{-3};

The average gas-liquid mass transfer coefficient and average specific area of bubbles can be correlated by equations (Garcia-Ochoa and Gomez, 2004):

$$k_L = \frac{2}{\sqrt{\pi}}\sqrt{D_{CO_2}}\left(\frac{\varepsilon\rho_L}{\mu_L}\right)^{1/4} \tag{17}$$

$$a_G = 6\varphi / d_b \tag{18}$$

where ρ_L and μ_L are the density and dynamic viscosity of liquid phase, kg· m^{-3} and Pa·s^{-1}; ε is average energy dissipation, w·kg^{-1}; α_G is the specific area of bubbles, m^2/m^3; φ is the gas hold up; d_b is the average diameter of bubbles, m.

In the liquid phase, dissolved CO_2 forms carbonate ions. This ionization affects the apparent solubility and must be taken into account. The equilibrium reactions are (Cents et al, 2005):

$$CO_2(l) + OH^- \xleftrightarrow{k_{11}/k_{12}} HCO_3^- \tag{19}$$

$$HCO_3^- + OH^- \xleftrightarrow{k_{21}/k_{22}} CO_3^{2-} + H_2O \tag{20}$$

$$H^+ + OH^- \xleftrightarrow{k_{31}/k_{32}} H_2O \tag{21}$$

$$CO_2(l) + H_2O \xleftrightarrow{k_{41}/k_{42}} HCO_3^- + H^+ \tag{22}$$

The expressions of reaction rates are:

$$r_1 = k_{11}[CO_2(l)][OH^-] - k_{12}[HCO_3^-] \tag{23}$$

$$r_2 = k_{21}[HCO_3^-][OH^-] - k_{22}[CO_3^{2-}] \tag{24}$$

$$r_3 = k_{31}[H^+][OH^-] - k_{32} \tag{25}$$

$$r_4 = k_{41}[CO_2(l)] - k_{42}[HCO_3^-][H^+] \tag{26}$$

where the k_{ij} are reaction rate constants, $m^3 \cdot mol^{-1} \cdot s^{-1}$, mol· $m^{-3} \cdot s^{-1}$ and s^{-1}.

2.3 The enhancement factor of mass transfer

The solid-liquid mass transfer and gas-liquid mass transfer can be enhanced by the second order chemical reaction between CO_2(l) and OH^- in the liquid film near the solid-liquid interface and gas-liquid interface (Uchida et al., 1975). This phenomenon can be described by the enhancement factor E (van Krevelen and Hoftijzer, 1948):

$$E_A = \frac{\left[M_{reaction}(E_i - E_A)/(E_i - 1)\right]^{1/2}}{\tanh\left[M_{reaction}(E_i - E_A)/(E_i - 1)\right]^{1/2}} \tag{27}$$

where E_A is the enhancement factor for second order chemical reaction; E_i is the asymptotic enhancement factor for the same reaction in the instantaneous regime; $M_{reaction}$ is the reaction parameter. E_i and $M_{reaction}$ can be calculated as follow:

$$E_i = \left(1 + \frac{c_B^b D_B}{b c_A^i D_A}\right) \tag{28}$$

$$M_{reaction} = \frac{D_A k_r c_B^b}{\left(k_f\right)^2} \tag{29}$$

where c_B^b is the concentration of component B in the bulk solution, $mol \cdot m^{-3}$; c_A^i is the equilibrium concentration of component A on the interface, $mol \cdot m^{-3}$; D_A and D_B are the diffusion coefficient of components, $m^2 \cdot s^{-1}$; k_r is the second order chemical reaction rate constant, $m^3 \cdot mol^{-1} \cdot s^{-1}$; k_f are solid-liquid mass transfer coefficient (k_s) near the solid phase and gas-liquid mass transfer coefficient (k_L) near the gas phase, $m \cdot s^{-1}$.

The enhancement factor above is derived by assuming instantaneous reaction. The reaction between CO_2(l) and OH^- in the liquid film has been calculated by the diffusion-reaction model based on the real physical boundary conditions. Almost all of the OH^- is consumed by the reaction in the liquid film near the solid-liquid interface. Therefore, the film reaction can be assumed fast. The solid-liquid mass transfer and gas-liquid mass transfer can be expressed as:

$$N_{i,sL} = k_{s,i} E_{sL} \Delta c_i - k_{s,i} E_{sL} z_i \overline{c_i} \left[\frac{\sum_i (z_i k_{s,i} \Delta c_i)}{\sum_i (z_i^{\,2} k_{s,i} \overline{c_i})} \right] \tag{30}$$

$$N_{CO_2,gL} = k_L E_{gL} \left[\left(\frac{H_{CO_2-H_2O} M_{CO_2} [CO_2(g)]_{IN} P}{\rho_{CO_2}} \right) - [CO_2(l)] \right] \tag{31}$$

where E_{sL} and E_{gL} are the enhancement factors of solid-liquid and gas-liquid mass transfer; $N_{i,sL}$ and $N_{CO2,gL}$ are the enhanced fluxes respectively.

Although the enhancement factor approach above is strictly valid only for cases where bulk phase concentration is negligible, the above equation can be used in practice with driving force Δc_i defined in a traditional way. The reason for this is that whenever the enhancement factor deviates significantly from unity, the bulk phase concentrations are anyway very small due to fast reaction rates and the above equation reduces to the classical enhancement factor formulation (Danckwerts, 1970). When reaction rate is relatively slow, the above equation reduces to the classical mass transfer model as the enhancement factor is unity. Although in between these limiting cases the formulation is not strictly correct, the deviation from precise intermediate reaction rate profiles is minor. In this way, a single equation can be used both for fast and moderate reaction rate regimes without a need to switch between different mass transfer models.

2.4 Precipitation Model

In this study, the precipitation of magnesium carbonate was given by:

$$Mg^{2+} + CO_3^{\,2-} \rightarrow MgCO_3(s) \tag{32}$$

In the precipitation model, supersaturation, nucleation, size-independent crystal growth and the first four moments (μ_0, μ_1, μ_2, μ_3) were taken into account in the population balance equation. The nucleation and crystal growth rates were calculated by power-law functions (Nielsen, 1964):

$$B = k_n (S)^n \tag{33}$$

$$G = k_g (S)^g \tag{34}$$

where B is the nucleation rate, #· m^{-3}·s^{-1}; G is the growth rate, m·s^{-1}; k_n is the nucleation rate constant, mol^{-n}·$m^{(3n-3)}$ ·s^{-1}; k_g is the growth rate constant, mol^{-g}·$m^{(3g+1)}$·s^{-1}; n, g are exponent of nucleation and growth respectively. S is the supersaturation in the bulk solution (Rigopoulos and Jones, 2001):

$$S = \sqrt{[Mg^{2+}][CO_3^{2-}]} - \sqrt{K_{sp,MgCO_3}} \tag{35}$$

The general population balance equation for semi-batch precipitation system is (Randolph and Larson, 1988; Wachi and Jones, 1992):

$$\frac{\partial n(L)}{\partial t} + \frac{\partial (Gn(L))}{\partial L} = B(n(L)) - D(n(L)) \tag{36}$$

This formulation of the population balance equation is valid for the semi-batch processes with constant volume. The volume expansion due to the feeding gas is relatively small compared to the volume of liquid. Therefore, the total volume of solution can be assumed to be constant in this work. For semi-batch processes with feeding with liquid solution, the "dilution" effect should be included.

According to the above assumptions, the PBE can be simplified and expressed as:

$$\frac{\partial n(L)}{\partial t} + G\frac{\partial n(L)}{\partial L} = 0 \tag{37}$$

where $n(L)$ is the number density related to the size of the crystal L, m^{-4}; $B(n(L))$ and $D(n(L))$ are birth and death functions.

In order to transform the PDEs into ODEs, the moment transformation was introduced as follows (Randolph and Larson, 1988; Jones et al., 1992):

$$\mu_j = \int_0^\infty n(L)L^j dL \tag{38}$$

$$\frac{d\mu_j}{dt} = jG\mu_{j-1} + L_0{}^j B \quad (j = 0,1,2,3) \tag{39}$$

where μ_j is the j^{th} moment of the crystal distribution, m^{j-3}. L_0 is the primary nucleate crystal dimension, m. The crystal mass deposition rate due to the nucleation and crystal growth, D_B and D_G:

$$D_B = \alpha\rho_{MgCO_3} L_0{}^3 B \tag{40}$$

$$D_G = \beta\rho_{MgCO_3}\mu_2 G/2 \tag{41}$$

where α and β are volume shape factor and surface shape factor . For spherical particles, they are $\pi/6$ and π respectively.

Based on the above considerations, the comprehensive model including dissolution, absorption and precipitation can be used to describe the heterogeneous precipitation:

$$\frac{d[CO_2(l)]}{dt} = N_{CO_2,gL}\alpha_G V_{disp}/V_L - r_1 - r_4 \tag{42}$$

$$\frac{d[OH^-]}{dt} = N_{OH,sL}\alpha_S V_{disp}/V_L - r_1 - r_2 - r_3 \tag{43}$$

$$\frac{d[H^+]}{dt} = N_{H,sL}\alpha_S V_{disp}/V_L - r_3 + r_4 \tag{44}$$

$$\frac{d[HCO_3^-]}{dt} = r_1 - r_2 + r_4 \tag{45}$$

$$\frac{d[CO_3^{2-}]}{dt} = r_2 - D_B - D_G \tag{46}$$

$$\frac{d[Mg^{2+}]}{dt} = N_{Mg,sL}\alpha_S V_{disp}/V_L - D_B - D_G \tag{47}$$

$$\frac{dn_{Mg(OH)_2}}{dt} = -N_{Mg,sL}\alpha_S V_{disp} \tag{48}$$

$$\frac{d\mu_j}{dt} = jG\mu_{j-1} + L_0{}^j B(j = 0,1,2,3) \tag{49}$$

The values of the reaction rate constants and physical parameters used in the above models are summarized in Table 1 (Cents et al, 2005).

Table 1
Physical and reaction kinetics parameters.

Parameter	Value	Unit	Parameter	Value	Unit
D_{Mg2+}	7.06×10^{-10}	$m^2\cdot s^{-1}$	k_{11}	1.41×10	$m^3\cdot mol^{-1}\cdot s^{-1}$
D_{H+}	9.21×10^{-9}	$m^2\cdot s^{-1}$	k_{12}	3.11×10^{-4}	s^{-1}
D_{OH-}	5.17×10^{-9}	$m^2\cdot s^{-1}$	k_{21}	6.00×10^{6}	$m^3\cdot mol^{-1}\cdot s^{-1}$
$D_{CO2(l)}$	1.59×10^{-9}	$m^2\cdot s^{-1}$	k_{22}	1.22×10^{6}	s^{-1}
$\rho_{Mg(OH)2}$	2.34×10^{3}	$kg\cdot m^{-3}$	k_{31}	1.40×10^{8}	$m^3\cdot mol^{-1}\cdot s^{-1}$
ρ_{MgCO3}	2.96×10^{3}	$kg\cdot m^{-3}$	k_{32}	1.29	$mol\cdot m^{-3}\cdot s^{-1}$
ρ_{CO2}	1.80	$kg\cdot m^{-3}$	k_{41}	2.40×10^{-2}	s^{-1}
H	35	$mol\cdot m^{-3}\cdot atm^{-1}$	k_{42}	5.70×10	$m^3\cdot mol^{-1}\cdot s^{-1}$
α	$\pi/6$	dimensionless			
θ	π	dimensionless			

3 Results and discussion

3.1 Experimental apparatus and initial input parameters

The experimental results of the precipitation with $Mg(OH)_2$(s)-CO_2(g)-H_2O(l) multiphase system have been reported in the literature (Han et al., 2014a, 2014b). The concentration of magnesium ($[Mg^{2+}]$) was measured by ion chromatography (ICS-1100 from Thermo Scientific Inc.). The mass fraction of $Mg(OH)_2$ in the solids was analyzed by the thermal measurements, thermogravimetry (TG) and differential scanning calorimetry (DSC) because the dissolving particles and crystals of $MgCO_3$ coexisted in the mixture during the precipitation. To obtain the solid-liquid mass transfer coefficient in the model, the impeller input power needs to be calculated based on the dimension of experimental apparatus and the initial input parameters in Table 2 (Han et al., 2014b).

Table 2
Dimension of experimental apparatus and the initial input parameters.

Parameter	Value	Unit	Parameter	Value	Unit
$D_{impeller}$	5.4×10^{-2}	m	Q_g	1.67×10^{-5}, 1.50×10^{-4}	$m^3\cdot s^{-1}$
$H_{impeller}$	1.0×10^{-2}	m	N	560, 650	rpm
D_{tank}	1.5×10^{-1}	m	$n_{Mg(OH)2}$	1.71	mol
V_L	2.5×10^{-3}	m^3	d_p	2.64×10^{-5}	m
T	298	K	P	1	atm

From the presented model of precipitation, the concentration of each component in the liquid phase and the amount of solid reactant and product can be obtained at different operating conditions. However, the rate constant and exponent of nucleation and crystal growth of $MgCO_3$ have not been reported in the previous studies. The kinetic parameters for $CaCO_3$ were used first to test the model (Hostomský and Jones, 1995). Then, the parameters for $MgCO_3$ (k_n, k_g, n, g) were fitted against the experimental data by the least square method (lsqnonlin function) in Matlab R2014a. In the literature, the nucleation constant (k_n) was typically fitted separately for each operating condition because the nucleation is sensitive to the geometry and mixing conditions in the stirred tank reactor (Myerson, 2001). This approach is also followed here, although later a tentative dependency on the operating conditions is proposed.

3.2 The effect of impeller speed (N) and gas flow rate (Q_g)

The concentration of magnesium ([Mg^{2+}]) is presented in Fig. 1(a). It shows that [Mg^{2+}] increases gradually at the beginning. After reaching a peak value, [Mg^{2+}] decreases substantially and tends to slow down at the end of the process. The mass fraction of $Mg(OH)_2$ in the mixture is shown in Table 3 (Han et al, 2014a). According to the concentration of magnesium in the liquid phase and the mass fraction of $Mg(OH)_2$, the amount of $Mg(OH)_2$ and $MgCO_3$ are calculated independently in Fig. 1(b) and Fig. 1(c). The solids of $Mg(OH)_2$ dissolve gradually during the whole precipitation. The crystals of $MgCO_3$ start to precipitate after the [Mg^{2+}] reaches the peak value.

Table 3
Mass fraction of $Mg(OH)_2$ in the solid mixture.

N = 560 rpm $Q_g = 1.67\times10^{-5}\ m^3\cdot s^{-1}$		N = 560 rpm $Q_g = 1.50\times10^{-4}\ m^3\cdot s^{-1}$		N = 650 rpm $Q_g = 1.67\times10^{-5}\ m^3\cdot s^{-1}$	
Time, min	Mass fraction, wt%	Time, min	Mass fraction, wt%	Time, min	Mass fraction, wt%
0	100	0	100	0	1
5	94.77	5	97.01	5	96.99
10	95.32	13	92.15	10	88.87
20	92.31	20	84.62	15	86.68
30	76.09	30	25.99	20	84.54
50	2.23	50	0	50	0.82

The influence of different operating conditions on the overall reaction rate and yield of crystals is shown in Fig. 1. Higher impeller speed and gas flow rate improve the dissolution and precipitation rate significantly. The gas flow rate presents stronger effect on the overall reaction rate than impeller speed in this work.

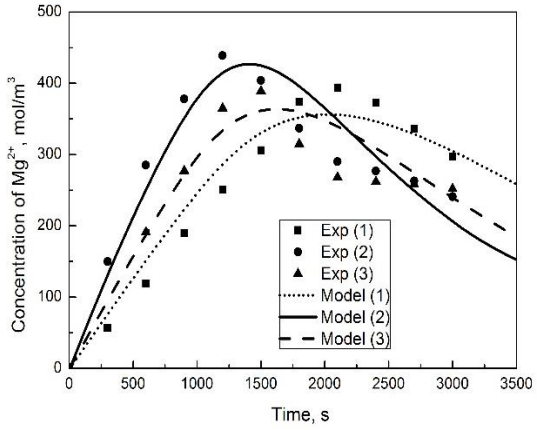

(a) Concentration of Mg^{2+}.

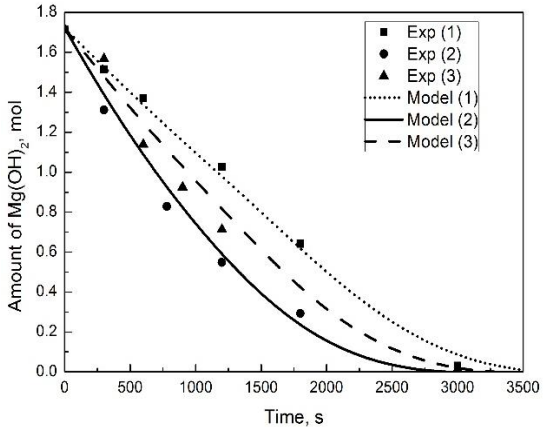

(b) Amount of $Mg(OH)_2$.

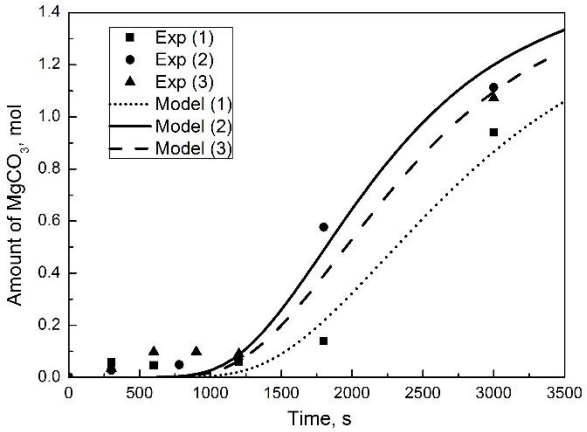

(c) Mass of $MgCO_3$.

Fig.1. Modeling vs experimental results from Han et al. (2014b): Exp (1) and Model (1): N = 560 rpm, $Q_g = 1.67\times10^{-5}$ $m^3\cdot s^{-1}$; Exp (2) and Model (2): N = 560 rpm, $Q_g = 1.50\times10^{-4}$ $m^3\cdot s^{-1}$; Exp (3) and Model (3): N = 650 rpm, $Q_g = 1.677\times10^{-5}$ $m^3\cdot s^{-1}$.

Three distinctive periods can be deduced according to the experimental and modelling results. The first one is the induction which introduces supersaturation and nucleation. The magnesium and carbonate ions are produced by the dissolution of $Mg(OH)_2$ and absorption of CO_2. The consumption of $[Mg^{2+}]$ is insignificant compared to the accumulation because the volume of crystal nucleus is quite small. The model assumes that the amount of nucleus has weak contribution to the amount of $MgCO_3$ during the induction, which explains the small deviation between the modeling and experimental result in Fig. 1 (c) during the first 1000s. Another reason is that the higher local supersaturation near the gas sparger may lead to burst nucleation during the induction period. The second period is growth of the nucleus. Once the nucleus reaches a critical level, concentration of magnesium decreases sharply due to the high supersaturation and the following growth of nucleus. The amount of $MgCO_3$ begins to accumulate during the growth period as shown in Fig. 1 (c). The last of the three periods is the equilibrium period. The supersaturation produced by the magnesium and carbonate ions is not high enough for further precipitation. The precipitation rate displays a deceasing tendency at the end of precipitation. The $[Mg^{2+}]$ tends to remain at a relatively high value. It is interesting to note that the dissolution rate tends to slow down during the crystal growth period in Fig. 1 (b).

The liquid-solid and gas-liquid mass transfer influence the global rate of precipitation considerably. The higher impeller speed leads to the increase of average energy dissipation in the stirred tank. Consequently, the higher mass transfer coefficient in proportion to the energy dissipation accelerates overall rate of dissolution and absorption. Meanwhile, the higher impeller speed and gas flow rate can also improve the breakage of bubbles and increase the mass transfer area between gas and liquid phases. In the crystal growth period, the deviation between modeling and experimental results may be caused by the non-ideal mixing conditions in Fig. 1 (a). The consumption rate of [Mg^{2+}] turns to be sensitive to the distribution of supersaturation during the growth of crystals. According to the experimental observation, almost no gas exists under the gas sparger in the tank. Therefore, the local supersaturation could be different from the average value calculated by the model. Further model development with fluid dynamic considerations will be needed to analyze this in the future.

3.3 The effect of pH and enhancement factor (*E*)

The experimental result and the prediction of pH are shown in Fig. 2(a). The pH drops sharply at the first few seconds and then decreases gradually during the precipitation. The pH is a key parameter which dominates the main species including CO_2(l), HCO_3^- and CO_3^{2-} in the CO_2(g)-H_2O(l) equilibrium system. The concentration of carbonate, [CO_3^{2-}], magnesium, [Mg^{2+}] and supersaturation of the system are shown in Fig. 2(b). [CO_3^{2-}] begins to reduce when pH is lower than 8.5 and remains at relatively low value at the end of precipitation. It shows that [CO_3^{2-}] has a stronger effect than [Mg^{2+}] on the supersaturation. The nucleation and growth of crystal tends to slow down due to the decreasing surpersaturation. Therefore, [Mg^{2+}] remains at relatively high value even under further introduction of carbon dioxide. In order to improve the utilization of magnesium and the yield of precipitation, the sodium hydroxide solution can be introduced into the precipitation system (Mitsuhashi et al. 2005).

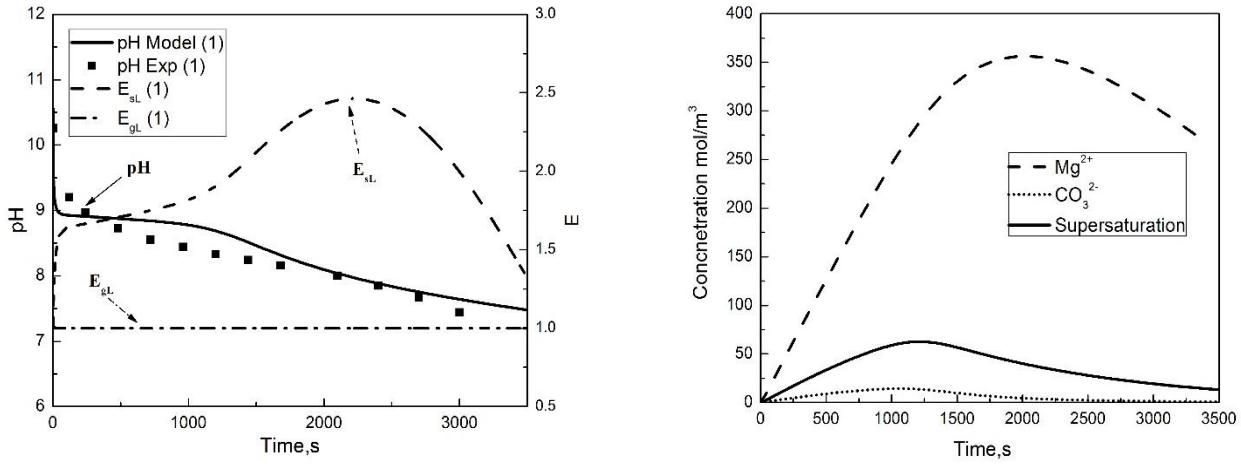

(a) pH and Enhancement factor

(b) Concentration of components and supersaturation

Fig.2. pH, enhancement factor, concentration of components and supersaturature, Exp (1) and Model (1): N = 560 rpm, $Q_g = 1.67\times10^{-5}\ m^3\cdot s^{-1}$.

In addition, the pH is one of the reasons which lead to nucleation in the electrolyte solution. Electrical interaction between clusters or nucleus has an important influence on aggregation of nucleus and stability of crystals. The isoelectric point is the pH at which the solids carry no net electrical charge. The attraction or repulsion force between particles exists when the pH of aqueous system deviates from the isoelectric point. It is likely that, therefore, nucleation will happen near the isoelectric point due to the weak repulsion force between similar nucleuses. The isoelectric point of $MgCO_3$ is 8.5 (Pokrovsky et al., 1999). It shows that the induction period mainly exists within the first 1000s near the isoelectric point.

The enhancement factors for solid-liquid mass transfer (E_{sL}) and gas-liquid mass transfer (E_{gL}) are shown in Fig. 2(a). The enhancement factors are controlled by the bulk concentration of components and the thickness of the liquid film near the surfaces of solids and bubbles. For the solid-liquid mass transfer, E_{sL} increases at the beginning of precipitation. The reaction between CO_2(l) and OH^- in the liquid film improve the mass transfer rate near the solid-liquid interface. Meanwhile, the decrease of the thickness of the liquid film due to the shrinking diameter of particle will limit E_{sL}. After the diameter of $Mg(OH)_2$ reduces to certain level, the limitation on the E_{sL} becomes more significant. This happens at around 2300s in the modeled precipitation

process. Therefore, the dissolution rate tends to slow down because of the decreasing E_{sL} at the end of precipitation in Fig. 1 (b). For the gas-liquid mass transfer, E_{gL} remains at 1 during the absorption of CO_2. The bulk concentration of OH^- drops immediately at the beginning of precipitation. E_{gL} can be ignored in the gas-liquid mass transfer due to the low concentration of OH^- in the solution.

3.4 The effect of precipitation kinetics and volumetric gas-liquid mass transfer coefficient (k_La)

It is interesting to compare the present model results with precipitation kinetics of other chemically similar systems. One such is production of $CaCO_3$ particles, for which a precipitation model is available in the literature (Hostomský and Jones, 1995). In order to ease the comparison, the same gas flow and mixing conditions were used in simulation of $CaCO_3$ system as in the present $MgCO_3$ case. The simulation results with different precipitation kinetics parameters (Table 4) are shown in Fig. 3 (a), (b) and (c). 95% confidence limits are presented for our parameter fitting for $MgCO_3$. Unfortunately, confidence limits were not reported for $CaCO_3$ precipitation in the literature.

Table 4
Comparison between precipitation coefficients of $CaCO_3$ (Hostomský and Jones, 1995) and $MgCO_3$

Precipitation kinetics of $CaCO_3$			Precipitation kinetics of $MgCO_3$ (This study)		
Parameter	Value	Unit	Parameter	Value	Unit
k_n	9.00×10^{9}	$mol^{-n}\cdot m^{(3n-3)}\cdot s^{-1}$	k_n (Model 1)	$(9.73\pm0.06)\times10^{6}$	$mol^{-n}\cdot m^{(3n-3)}\cdot s^{-1}$
k_g	5.50×10^{-9}	$mol^{-g}\cdot m^{(3g+1)}\cdot s^{-1}$	k_n (Model 2)	$(5.69\pm0.03)\times10^{7}$	$mol^{-n}\cdot m^{(3n-3)}\cdot s^{-1}$
n	8.60	dimensionless	k_n (Model 3)	$(3.37\pm0.04)\times10^{7}$	$mol^{-n}\cdot m^{(3n-3)}\cdot s^{-1}$
g	2.00	dimensionless	k_g	$(1.02\pm0.05)\times10^{-10}$	$mol^{-g}\cdot m^{(3g+1)}\cdot s^{-1}$
			n	(1.11 ± 0.04)	dimensionless
			g	(1.29 ± 0.09)	dimensionless

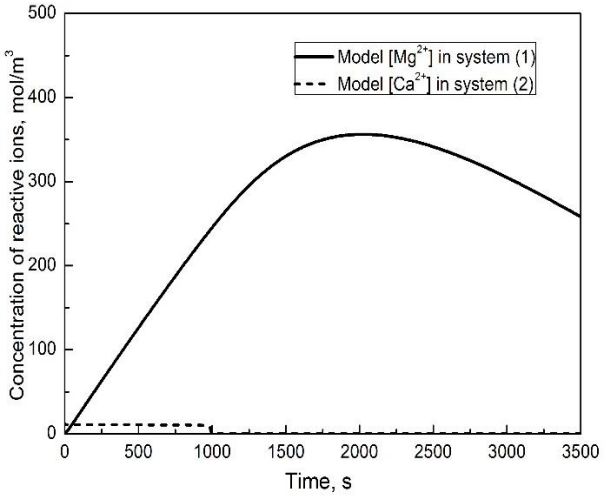

(a) Concentration of reactive ions.

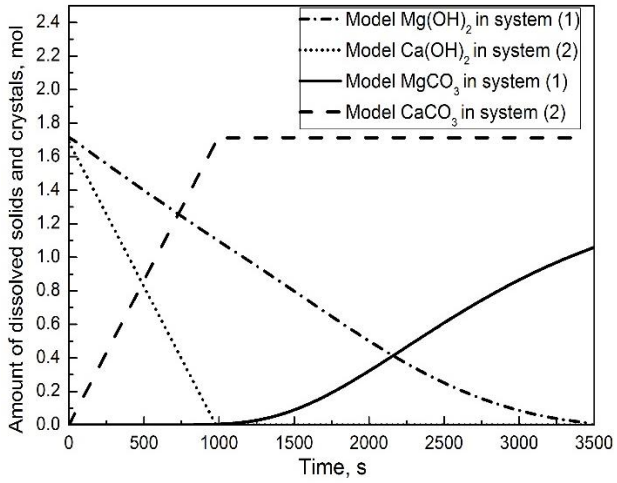

(b) Amount of dissolving particles and crystals.

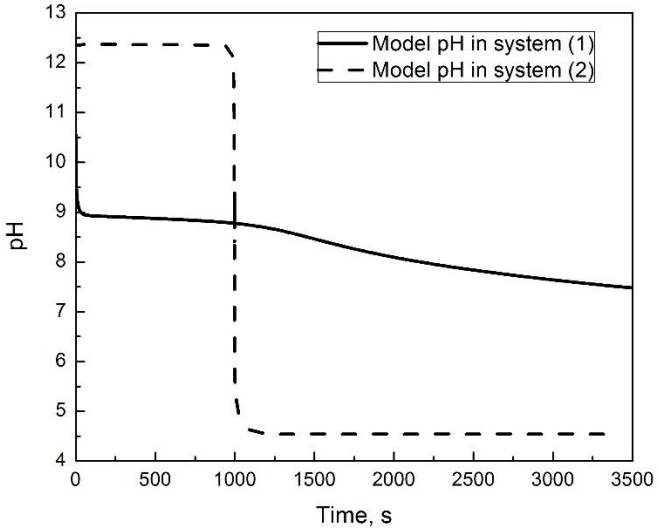

(c) pH.

Fig.3. Comparison between precipitation systems. System (1): $Mg(OH)_2$ (s)+CO_2 (g)+H_2O (l); System (2): $Ca(OH)_2$ (s)+CO_2 (g)+H_2O (l). Operating conditions: N = 560 rpm. $Q_g = 1.67\times10^{-5}$ $m^3\cdot s^{-1}$.

The accumulated concentration of reactive ions of calcium is much lower than magnesium. However, the yield of crystals in the calcium system is higher than that in the magnesium system. The rate of dissolution and precipitation in the calcium system is also faster than that in the magnesium system. The comparison of precipitation kinetics in table 4 indicates that the nucleation rate and crystal growth rate of $MgCO_3$ is remarkably lower than the $CaCO_3$, which leads the differences in accumulated concentration of reactive ions and the yield of crystals in Fig. 3(a) and (b). The modeling result of calcium system is similar with previous studies on gas-liquid precipitation (Han et al., 2014a; Rigopoulos and Jones, 2001). The difference of

dissolution rate can be explained based on the solubility of reactant solids. The solubility product of $Ca(OH)_2$ (K_{sp} = 5.5 ×10^3) is ten thousand times higher than that of $Mg(OH)_2$ (K_{sp} = 1.8 ×10^{-2}) at 25°C in water (Hill et al., 2004). It's easier for $Ca(OH)_2$ to dissolve in the CO_2-H_2O system than $Mg(OH)_2$. The reactive dissolution can improve the absorption rate of CO_2 reversely which has a strong influence on the precipitation rate. Therefore, the concentration of Ca^{2+} reaches the highest value before Mg^{2+} in Fig. 3 (a) while the amount of $CaCO_3$ also increase rapidly before $MgCO_3$ in Fig. 3 (b). In addition, the pH of calcium system remains at 12.35 during the precipitation because the reaction between CO_2(l) and OH^- mainly occurs in the liquid film near the gas-liquid interface in Fig. 3 (c). For calcium system, the enhancement factor (E_{gL}) for the gas-liquid mass transfer is 1.16 due to the high concentration of OH^- while the enhancement factor (E_{sL}) for the solid-liquid mass transfer can be ignored. The higher pH produces higher [CO_3^{2-}] for the calcium system than magnesium system. Consequently, the rate of nucleation and growth of $CaCO_3$ is faster than $MgCO_3$. The induction period of calcium system is not obvious any more.

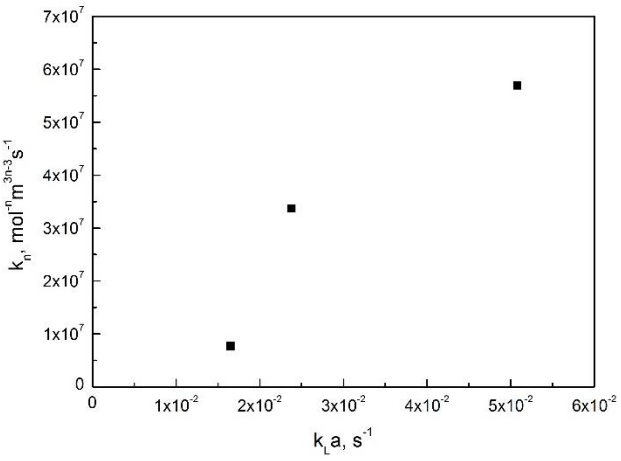

Fig.4. The relation between nucleation constant and the volumetric gas-liquid mass transfer coefficient

In the present work, the nucleation constant (k_n) was fitted individually for each operating condition. Although the nucleation rate is typically very unpredictable, in the present cases there seems to be a clear trend between primary nucleation rate and volumetric mass transfer coefficient, as shown in Fig.4. The trend seems almost linear, and actually the simulation results would be almost equally good if a strict linear dependency would be assumed. The supersaturation which is the driving force of nucleation and crystal

growth depends on the concentration of Mg^{2+} and CO_3^{2-}. On one hand, absorption of CO_2 improves dissolution of magnesium hydroxide. On the other hand, the absorption can yield carbonate ion by itself. The increase of absorption will enhance the nucleation rate which leads to more fine crystals in the product. Therefore, the desired size of crystals can be obtained by controlling the absorption rate of CO_2(g).

In the view of the above discussion, the concentration of components and the final properties of crystals result from the mutual effect of the dissolution of the reactant particles, CO_2 absorption and precipitation during the whole precipitation. A mathematical model taking into account the three processes simultaneously is more reliable than the assumption of a single rate controlling step. A certain degree of deviation still exists between the concentration of magnesium from the experiment and mathematical model due to non-ideal mixing condition. It reveals the significance of the hydrodynamics in the research of heterogeneous precipitation. This model will be implemented into the computational fluid dynamics coupled with integrated population balance equation in the future work.

4 Conclusions

This paper proposes a mathematical model for the process of precipitation of magnesium carbonate in a heterogeneous stirred tank reactor. The model includes a description of dissolution, absorption and precipitation. In the dissolution model, the Nernst-Planck equation is introduced to ensure the mass balance and electroneutrality between the solid and liquid phases. The influence of the diameter of dissolving particles and the second order chemical film reaction on the mass transfer are taken into account in the dissolution model. In the precipitation model, a simplified population balance equation is solved by the moment transformation under ideal mixing assumption.

The present model is capable of predicting concentrations of reactive ions, pH of the solution and the amount of dissolving solids and precipitated crystals. The modeling results showed excellent agreement with the available experimental data with fitted crystallization kinetics. The gas-liquid and liquid-solid mass transfer

dominate the global rate of precipitation, and during the reactive precipitation several phenomena is rate limiting. Precipitation kinetics and pH determine the accumulated concentration of reactant and the yield of precipitation. The relation between the dissolution, absorption and precipitation can be analyzed based on the experimental and modeling results. The complex interaction reflects the need for combing the three processes in a comprehensive mathematical model.

Nomenclature

A	total mass transfer area, m^2
B	nucleation rate, $\#\cdot m^{-3}\cdot s^{-1}$
b	stoichiometric coefficient, dimensionless
c_i	concentration of component, $mol\cdot m^{-3}$
c^i	concentration of component on the interface, $mol\cdot m^{-3}$
c^b	concentration of component in the bulk solution, $mol\cdot m^{-3}$
d_p	average diameter of particles, m
d_b	average diameter of bubbles, m
D_B	crystal mass deposition rate due to nucleation, $mol\cdot m^{-3}\cdot s^{-1}$
D_G	crystal mass deposition rate due to crystal growth, $mol\cdot m^{-3}\cdot s^{-1}$
D_i	diffusion coefficient, $m^2\cdot s^{-1}$
$D_{impeller}$	diameter of the impeller, m
D_{tank}	diameter of the tank, m
E_{sL}	enhancement factor for the solid-liquid mass transfer, dimensionless
E_{gL}	enhancement factor for the gas-liquid mass transfer, dimensionless
E_i	asymptotic enhancement factor in the instantaneous regime, dimensionless
F	Faraday constant, $C\cdot mol^{-1}$
g	exponent of growth, dimensionless
G	growth rate, $m\cdot s^{-1}$
$H_{CO2\text{-}H2O}$	Henry's constant, $mol\cdot m^{-3}\cdot atm^{-1}$
$H_{impeller}$	hight of the blade of the impeller, m
k_{ij}	first order reaction rate constant, $m^3\cdot mol^{-1}\cdot s^{-1}$ and s^{-1}
k_f	mass transfer coefficient, $m\cdot s^{-1}$
k_g	growth rate constant, $mol^{-g}\cdot m^{(3g+1)}\cdot s^{-1}$
k_n	nucleation rate constant, $mol^{-n}\cdot m^{(3n-3)}\cdot s^{-1}$
k_L	gas-liquid mass transfer coefficient, $m\cdot s^{-1}$
$k_{s,i}$	solid-liquid mass transfer coefficient, $m\cdot s^{-1}$
k_r	second order chemical reaction rate constant, $m^3\cdot mol^{-1}\cdot s^{-1}$
K_{sp}	solubility product, $mol^2\cdot m^{-6}$
L_0	effective crystal dimension, m
$M_{Mg(OH)2}$	molar mass of $Mg(OH)_2$, $kg\cdot mol^{-1}$
$M_{reaction}$	chemical reaction parameter, dimensionless
n	exponent of nucleation, dimensionless
$n_{Mg(OH)2}$	total number of moles of $Mg(OH)_2$, mol
$n(L)$	number density, m^{-4}
N	rate of the impeller, rpm
N_i	flux between solid and liquid phase, $mol\cdot m^{-2}\cdot s^{-1}$
N_{CO2}	flux between gas and liquid phase, $mol\cdot m^{-2}\cdot s^{-1}$
N_{Sh}	Sherwood number, dimensionless

N_{Re}	Reynolds number, dimensionless
N_{Sc}	Schmidt number, dimensionless
N_{tot}	total number of solids, dimensionless
P	pressure of the system, atm
Q_g	gas flow rate, $m^3 \cdot s^{-1}$
r_i	reaction rate constant, $mol \cdot m^{-3} \cdot s^{-1}$
R	gas constant, $J \cdot K^{-1} \cdot mol^{-1}$
S	supersaturation, $mol \cdot m^{-3}$
T	temperature, K
v	velocity of component between the interface and bulk solution, $m \cdot s^{-1}$
V_{disp}	total volume of dispersion system, m^3
V_G	volume of gas phase, m^3
V_L	volume of liquid phase, m^3
V_S	volume of solid phase, m^3
z_i	charge of cationic and anionic, dimensionless

Greek letters

α	volume shape factor, dimensionless
α_S	specific mass transfer area of $Mg(OH)_2$, m^2/m^3
α_G	specific mass transfer area of CO_2, m^2/m^3
β	surface shape factor, dimensionless
ρ	density, $g \cdot m^{-3}$
ε	total energy dissipation, $w \cdot kg^{-1}$
$\nabla\phi$	potential gradient, $J \cdot C^{-1} \cdot m^{-1}$
φ	gas hold up, dimensionless
δ	thickness of liquid film, m
μ_L	dynamic viscosity of liquid phase, $Pa \cdot s^{-1}$
μ_j	j^{th} moment, m^{j-3}

Acknowledgment

Financial support from the Finnish Academy, project FLUKI (no. 13259597) is gratefully acknowledged

References:

Ala-Kaila K. Modelling of mass transfer phenomena in pulp-water suspensions, Ph.D. Thesis. Helsinki University of Technology. ESPOO; 1998.

Al-Rashed MH, Jones AG. CFD modelling of gas-liquid precipitation, Chem Eng Sci 1999;54:4779-84.

Asai S, Konishi Y, Kajiwara T. Effect of sparged gas on mass transfer between fine particles and liquids in an agitated vessel. J Chem Eng JPN 1989;22(1):96-8.

Beenackers AACM, Vanswaajj WPM. Mass-transfer in gas-liquid slurry reactors. Chem Eng Sci 1993; 48(18):3109-39.

Bhaskarwar AN. On application of the method of kinetic invariants to the description of dissolution accompanied by a chemical-reaction. Chem Eng Commun 1988;72:25-34.

Cents AHG, Brilman DWF, Versteeg GF. CO_2 absorption in carbonate/bicarbonate solutions: The Danckwerts-criterion revisited. Chem Eng Sci 2005;60(21):5830-5.

Cheng JC, Yang C, Mao ZS. CFD-PBE simulation of premixed continuous precipitation incorporation nucleation and aggregation in a stirred tank with multi-class method. Chem Eng Sci 2012;68:469-80.

Danckwerts PV. Significance of liquid-film coefficients in gas absorption. Ind Eng Chem 1951;A3:1460-7.

Danckwerts PV. Gas-liquid reactions. 1st ed. New York: McGraw-Hill; 1970.

Dokoumetzidis A, Papadopoulou V, Macheras P. Analysis of dissolution data using modified versions of Noyes–Whitney equation and the Weibull function. Pharm Res 2006;23:256–61.
Garcia-Ochoa F, Gomez E. Theoretical prediction of gas–liquid mass transfer coefficient, specific area and hold-up in sparged stirred tanks. Chem Eng Sci 2004;59:2489–501.
Han B, Qu HY, Niemi H, Sha ZL, Louhi-Kultanen M. Mass transfer and kinetics study of heterogeneous semi-batch precipitation of magnesium carbonate, Chem Eng Technol. 2014a;37(8):1363-8.
Han B, Qu HY, Niemi H, Sha ZL, Louhi-Kultanen M. Mechanistic study of magnesium carbonate semibatch precipitation with meganesium hydroxide and CO_2. Ind Eng Chem Res 2014b;53(30):12077-82.
Hill JW, Petrucci RH, McCreary TW, Perry SS. General Chemistry. 4th ed. New Jersey: Prentice-Hall; 2004.
Hsu JP, Lin DL, Lin MJ. Dissolution of solid particles in liquids-A surface-layer model. Colloid Surface 1991;61:35-47.
Hostomský J, Jones AG. A penetration model of the gas–liquid precipitation of calcium carbonate crystals. Transactions of AIChE, 1995;73(A):241–5.
Jones AG, Hostomsky J, Li Z. On the effect of liquid mixing rate on primary crystal size during the gas-liquid precipitation of calcium carbonate. Chem Eng Sci 1992;47(13-14):3817-24.
Jones AG, Rigopoulos S, Zauner R. Crystallization and precipitation engineering. Comp Chem Eng 2005;29: 1159-66.
Joshi JB, Pandit AB, Sharma MM. Mechanically agitated gas-liquid reactors. Chem Eng Sci 1982;37:813-44.
Khoury N, Mauger JW, Howard S. Dissolution rate studies from a stationary disk/rotating fluid system. Pharm Res 1988;5:495-500.
Levenspiel O. Chemical Reaction Engineering. 3rd ed. New York: John Wiley & Sons, Inc; 2007.
Lin RY, Zhang JY, Bai YQ. Mass transfer of reactive crystallization in synthesizing calcite nanocrystal. Chem Eng Sci 2006;61(21):7019-28.
Macheras P, Iliadis A. Modelling in Biopharmaceutics, Pharmacokinetics and Pharmacodynamics: Homogeneous and Heterogeneous Approaches. 1st ed. New York: Springer; 2006.
Missel PJ, Stevens LE, Mauger JW. Dissolution of anecortave acetate in a cylindrical flow cell: Re-evaluation of convective diffusion/drug dissolution for sparingly soluble drugs. Pharm Drug Dev Technol 2004a;9:453-9.
Missel PJ, Stevens LE, Mauger JW. Re-examination of convective diffusion/drug dissolution in a laminar flow channel: accurate prediction of dissolution rate. Pharm Res 2004b;12:2300-6.
Mitsuhashi K, Tagami N, Tanabe K, Ohkubo T, Sakai H, Koishi M, Abe M. Synthesis of microtubes with a surface of "house of cards" structure via needlelike particles and control of their pore size. Langmuir 2005;21(8):3659-63.
Mullin JW. Crystallization. 4th ed. Oxford: Butterworth-Heinemann; 2001.
Myerson AS. Handbook of industrial crystallization. 2nd ed. Woburn: Butterworth-Heinemann; 2001.
Newman JS. Electrochemical systems. 1st ed. New Jersey: Prentice-Hall; 1991.
Nielsen AE. Kinetics of Precipitation. 1st ed. Oxford: Pergamon Press;1964.
Noyes AA, Whitney WR. The rate of solution of solid substances in their own solutions. J Am Chem Soc 1897;19:930-4.
Pohorecki R, Baldyga J. The effects of micromixing and manner of reactor feeding on precipitation in stirred tank reactor. Chem Eng Sci 1988;43(8):1949-54.
Pokrovsky OS, Schott J, Thomas F. Processes at the magnesium-bearing carbonates/solution interface. I. A surface speciation model for magnesite. Geochimica et Cosmochimica Acta 1999; 63(6): 863-80.
Ramachandran PA, Sharma MM. Absorption with fast reaction in a slurry containing sparingly soluble fine particles. Chem Eng Sci 1969;24:1681-6.
Randolph AD, Larson MA. Theory of particulate processes. 2nd ed. New York: Academic Press; 1988.
Riazi MR, Faghri A. Solid dissolution with first-order chemical reaction. Chem Eng Sci 1985;40(8):1601-3.
Rice RG, Jonea PJ. Complete dissolution of spherical-particles in free-fall. Chem Eng Sci 1979;34(6):847-52.
Rigopoulos S, Jones AG. Dynamic modelling of a bubble column for particle formation via a gas-liquid reaction. Chem Eng Sci 2001;56:6177-84.
Sada E, Kumazawa H, Aoyama M. Reaction kinetics and controls of size and shape of goethite fine particles in the production process by air oxidation of alkaline suspension of ferrous hydroxide. Chem Eng Commun 1988;71:73-82.

Sada E, Kumazawa H, Butt MA. Single gas absorption with reaction in a slurry containing fine particles. Chem Eng Sci 1977;32(10):1165-70.
Sidorov GV, Gluzman SS, Ivanova VM, Vulakh EL. Application of the method of kinetic invariants to the description of a multiphase process of organic synthesis. J Appl Chem USSR 1986;58:1781–4.
Uchida S, Koide K, Shindo M. Gas absorption with fast reaction into a slurry containing fine particles. Chem Eng Sci 1975;30:644-6.
van Krevelen DW, Hoftijzer PJ. Kinetics of gas-liquid reaction kinetics Part I. General theory. Rec. Trav. Chim. Pays-Bas 1948;67(7):563-86.
Velts O, Uibu M, Kallas J, Kuusik R. CO_2 mineral trapping: Modelling of calcium carbonate precipitation in a semi-batch reactor. Energy Procedia 2011;4:771-8.
Wachi S, Jones AG. Mass transfer with chemical reaction and precipitation. Chem Eng Sci 1991a;46(4): 1027-33.
Wachi S, Jones AG. Effect of gas-liquid mass transfer on crystal size distribution during the batch precipitation of calcium carbonate. Chem Eng Sci 1991b;46(12):3289-93.
Wachi S, Jones AG. Dynamic modelling of particle size distribution and degree of agglomeration during precipitation. Chem Eng Sci 1992;47(12):3145-8.
Wang L, Fox RO. Application on in situ adaptive tabulation to CFD simulation of nano-particle formation by precipitation. Chem Eng Sci 2003;58(19):4387-401.
Wei H, Garsude J. Application of CFD modelling to precipitation systems. Chem Eng Res Des 1997;75(2): 219-27.